A new approach for strength and stiffness prediction of discontinuous fibre reinforced composites (DFC)

S.Z.H Shah[a], R.S Choudhry[b, *], Shuhaimi Mahadzir [c]

[a] Department of Mechanical Engineering, Universiti Teknologi PETRONAS, 32610 Bandar Seri Iskandar, Perak, Malaysia

[b] Department of Mechanical and Manufacturing Engineering, University of Derby, UK

[c] Centre for Process System Engineering, Institute of Autonomous Systems, Universiti Teknologi PETRONAS, 32610 Bandar Seri Iskandar, Perak, Malaysia

ABSTRACT

A new modelling methodology for strength and stiffness prediction of discontinuous fibre-reinforced composites (DFC) is proposed. This has been validated for both thermoplastic and thermoset, prepreg based, carbon fibre reinforced, random DFC laminates having high volume fraction, by implementing it in a commercial FE solver. The methodology involves explicit generation of internal architecture of DFC through an algorithm which is efficient (faster model generation and solution), easily customizable and scalable. It captures many of the realistic features of the DFC such as variation in volume fraction, interlacing of strands, random orientation and thickness variation of strands. Thus, the model accounts for the natural mechanical property variation, which is characteristic of random DFCs and was found to be conservative in terms of prediction of tensile strength and stiffness for all the validation cases considered. It is generic in the sense that it can be easily extended to generate preferentially aligned and hybrid DFC laminates.

Keywords: A. Discontinuous reinforcement; B. Mechanical properties; C. Finite element analysis (FEA); C. Micro-mechanics; Embedded finite element

Abbreviations: FEA, Finite element analysis; DFC, Discontinuous fibre-reinforced composites; FRC, Fibre reinforced composites; CLT, Classical laminate theory; RVE, Representative volume element; COV, Coefficient of variance; SAT, Separate axis theorem; UD, Unidirectional composite; QI, Quasi isotropic laminate;

1. Introduction

The prepregs or pre-impregnated FRC are widely used, for the manufacture of high-performance composite parts. Some of the reasons for this preference include, i) higher achievable volume fraction, ii) tighter control and repeatability of volume fraction and void content, iii) ease of automation using robotic tape layups that can also potentially speed up production [1]. The composite industry has been using continuous fibre prepregs for more than four decades due to their excellent properties; however, these composites have poor formability and

may suffer from wrinkling defect [2, 3]. This is particularly true for parts with complex curvature. One way to overcome this drawback is by using the prepreg based discontinuous fibre composites, as they possess excellent formability [4]. The mechanical properties of these composites are good, especially when the length of the fibres is greater than the critical fibre length [5]. Mathematically the maximum reinforcement efficiency of DFC can be achieved when the length of the fibres exceeds fifty times the critical fibre length [6].

The prepreg based discontinuous fibre composites in the form of mats and preforms have been used in the automotive and aerospace industry for the manufacturing of suspension arms, helicopter door hinges and 787 Dreamliner window frame [4, 7, 8]. These composites are available commercially from several manufacturers; such as HexMC® and Lytex® 4149 by Hexcel and Quantum respectively. They are manufactured using unidirectional prepregs, which are cut into 25-50 mm long strands. These strands are then randomly distributed and compressed into sheets, which are generally 2 mm thick but can be thinner or thicker depending upon the requirement. These materials combine the formability of discontinuous fibre reinforced composite and mechanical properties of high-performance continuous fibre reinforced composites [9]. In addition to this DFC, the material provides a sustainability solution for the composites industry as these can be produced from recycled fibre and thus reduce the composite manufacturing waste by transforming them into a valuable product [10, 11].

Properties of DFC depend on the many factors such as strands length, the thickness of strands, in-plane and out-of-plane orientation of strands [12-16]. These materials usually show a greater scatter in mechanical properties due to their random architecture and relatively smaller length of fibres [17-20]. Thus, a large number of experiments are required for generating design data, making mechanical property characterization expensive and challenging. This factor has contributed to relatively lesser use of DFC composites. As a response, several researchers presented analytical [18, 19, 21, 22] and numerical models [23, 24] to predict mechanical properties of DFC material.

Earlier models like Halpin and Pagano [21, 25] were based on CLT. These were originally proposed to model random fiber composites and not just prepreg based DFC's, and can be used to estimate the in-plane stiffness. The accuracy is limited however, because the size of strands is not considered. Feraboli et al. [19] proposed modified Halpin and Pagano [21] model to predict tensile modulus of DFC material by considering different strand sizes. They, however, considered only the in-plane orientation of strands. More recently, Nakashima et al. [18] proposed an analytical model to predict the flexure modulus of ultra-thin DFC. The proposed model captured the variation in the flexure modulus and accurately predicts the flexure strength. Although the

model was effective it was only validated for ultra-thin laminates where through thickness effects are not important.

In terms of strength prediction, Selezneva et al. [22] proposed an analytical model to predict strength and failure modes. This model does not account for the out of plane orientation of strands as well as the resin-rich areas. Consequently, it overpredicts the strength of DFC. A more accurate but semi-empirical model was proposed recently by Visweswaraiah et al. [26]. This is based on interlaminar shear and bending stress distribution to predict the strength of hybrid DFC. The authors found that Skin/DFC/Skin configuration gives the highest shear strength (25% higher). More recently, Li and Pimenta [27] have advanced the stochastic equivalent laminate analogy of Feraboli et al. [19] and proposed a multiscale model that uses analytical physically based failure criteria to predict strength and stiffness of tow-based DFCs while accounting for discontinuities in material architecture. In terms of analytical models this is perhaps one of the most comprehensive so far. It still, however, needs a larger data set for fuller validation and does not account for features such as out of plane bending (kinking) of tows (strands) and change of tow thickness and resin rich pockets in different regions of DFC.

In addition to analytical models, few authors have also used the FE method to predict the properties of DFC materials. While analytical models are faster and more suitable for producing general trends in property prediction they may be limited by the accuracy of underlying assumptions and requirement of parametrs which are hard to measure physically. It is also not easy to apply these to complex structures unless used in a multi-scale modelling framework. The FE models on the other hand offer the advantage that the methodology once validated can be easily automated and extended to any size of component (given that computaional resources are available), even if the user is not an expert of the underlying theory. The accuracy of the FE models however, depends strongly on the accuracy of the geometric model of internal architecture. A detailed literature review on strength/stiffness prediction of DFC presented by Visweswaraiah et al. [28] identified that the homogenized methodologies have been mostly adapted due to their ease in the implementation. However, these approaches overlooked geometrical effects (waviness) and process parameters (strands dimensions), which significantly influence the characteristics of DFC. The use of FE models that explicitly model the strand geometry thus opens up exciting opportunities for a more realistic predictions by better represnting the internal architecture. Generating the strand geometry and its distribution accurately and computationally efficiently is challenging, however. Similarly, defining the connection between these hundreds of strands and subsequently generating and solving a 3D continuous mesh is also computationally expensive for any reasonably sized part. Thus, in the next section we

have discussed these and other challenges, in the light of recent studies that utilize an explicit representation of internal architecture for FEA based prediction of properties of DFC composites.

2. Geometric Modelling Strategies of DFC material

As pointed out in the last section, the primary requirement for a good predictive model for characterization of DFC materials is a reasonably accurate geometric representation of the DFC material architecture. This is particularly important for high fibre volume fraction composites where the architecture contributes as significantly to the material properties as the volume fraction. Generating an accurate geometric representation which is representative of the in-plane as well as out-of-plane distribution is challenging, and simplified models based on conventional shell approaches often fail at that because these ignore the out-of-plane orientation of strands, defects due to voids, resin-rich areas, adhesion and interlaminar interaction between strands [19, 22].

The geometric models of DFC are broadly divided into three categories i.e. over-lapped geometric models, non-over-lapped in-plane geometric models, and non-over-lapped out-of-plane geometric models, as shown in Fig. 1. In overlapped geometric models each strand is shared between different cells and this does not represent the continuity of strands. On the other hand, non-over-lapped in-plane geometric models do not allow for representation of the true features of the high-volume fraction DFCs as observed in experiments. Thus, non-over-lapped out-of-plane geometric models have the potential to be most realistic. In this regards the work of Luchoo et al [29] was a good initial effort. He proposed a non-contact algorithm and spline interpolation to generate 3D architecture of fibre bundles. The main limitations of Luchoo's work were that it was firstly computationally expensive in terms of solution time. Secondly since 1D truss elements were used the input material behaviour for each tow had to be one-dimensional as well, which is not what is sufficient to model a prepreg strand based DFC where each strand can have a significant width requiring an orthotropic material definition and a non-circular cross-section. Thirdly although the spines of the fibre remained spaced there were possibilities of intersection elsewhere due to the use of circular cross-section profile.

The work of LT Harper et al. [30] significantly improved the earlier model and [29] used a force-directed algorithm to generate 3D architecture of DFC material. The author's considered out-of-plane orientation, bending and twisting of fibres bundles, and successfully generated RVE of small fibre bundles (3k having 1.7 mm width) with volume fraction close to 50%. However, for large fibre bundles (12k having 5.2 mm width) the author found significant intersection/penetration between strands with over 40% fibre volume fraction. This model was not specifically validated for the prepreg based DFC, although in theory it seems that one should be able to simply

replace tows with pre-preg strands. One limitation of this approach was a very long model generation time which could be 24 hours or more for a typical test coupon sized RVE.

Modelling DFC architecture as 3D solids offer some distinct advantages such as the ability to capture out-of-plane orientation of strands, waviness, resin-rich areas, interlaminar shear between strands and stress concentration effects. 3D solid architecture is, however, limited in terms of the maximum fibre volume fraction and required minimum clearance between strands to avoid element distortion issues in subsequent FE analysis. One such model was proposed by Pan at el. [31] where the authors used a random sequential algorithm to generate a three-dimensional solid architecture of randomly chopped fibre bundles. The authors found that with the in-plane orientation of fibre bundles the maximum fibre volume fraction achieved is 13.5%. However, by allowing the fibres to cross-over one another by introducing the out-of-plane orientation of fibres bundles, the fibre volume fraction could be increased up to 35%. Other limitations of this geometric model include an elliptic cross-section of fibre bundles, with fixed ratio between major and minor axis. One major disadvantage of such 3D models is the high model generation and computational cost due to the requirement of avoiding mesh intersections and a very large number of computationally expensive solid elements.

The review presented above indicates that the strategies used for geometric modelling and analysis of DFC material are inadequate. The main challenges in the geometric modelling of DFC material are; i) generating strands with random position and orientation while allowing for overlaps and avoiding intersection between strands, ii) maximizing the strand volume fraction to full fill the structural requirements iii) generating a geometric model that can lends itself to generate a computationally efficient FE mesh and iv) reducing the geometric model (RVE) generation time as much as possible to reduce the overall computation time. Thus, the proposed geometric model discussed in next section aims to overcome these challenges.

3. Proposed methodology

In this paper, we propose that the geometry of the individual discontinuous strands within an RVE of DFC composite being modelled using shell elements, and their material response being modelled using effective properties of an equivalent unidirectional reinforced composite. Depending on the type of DFC being modelled, i.e. aligned or random, the in-plane orientation of these strands (shells) can either be specified explicitly or assigned randomly in a prescribed range given by the user. We further propose that the out-of-plane orientations of strands being approximated using an automatically generated three-point interpolated path (spline) defined as a function of volume fraction, thickness of each layer within RVE and strand length. In order to avoid the problem of intersection we propose in this methodology, the use of separate axis theorem for interface detection between any two strands and to bring them as close as possible to generate a compact architecture of DFC. Finally, we

suggest that the strand architecture thus generated is embedded using embedded element technique in a solid element-based mesh which represents the matrix within the RVE. The use of embedded element technique with the proposed geometric modelling strategy results in a computationally efficient FE model that can be generated automatedly. In this paper we demonstrate the effectiveness and accuracy of this methodology by implementing it using Python code, within the ABAQUS, FE analysis software environment. Using this code, we generated four different architecture of DFC, i.e. random DFC, tailored DFC, aligned DFC and hybrid DFC. The model was validated by comparing the results of random DFC case with experimental data available in the literature. Details are presented in the following sections.

3.1. Details of geometric modelling of DFC

A code has been developed in Python and implemented in ABAQUS CAE to generate the architecture of DFC material. With this code, architectures of DFC material with variable strands dimension, orientation, specimen geometry and fibre volume fraction can be generated in a predefined RVE. In the geometry of DFC material, there is no repeated unit cell as in case of regular geometries; therefore, RVE approach is used, where the RVE may either be equivalent to structure dimensions or used with a sub-modelling approach for local-global analysis. In this study, the length of RVE is selected as at least one and half times the maximum length of strand that we used, so that maximum number of strands have their both ends inside the RVE and this is sufficient to represent the whole DFC architecture. In order to quantify the variability of properties from sample to sample, we generate five unique RVE for each test that we have virtually simulated. This point will be explained in more detail in the results section.

The geometric modelling approach used in this work is based on a non-over-lapped geometric model with out-of-plane orientation of strands, which is constrained within a layer. It is important to note that by allowing the fibres to bend and deflect out of plane (as happens in real composites [12], [15]) allows for a more realistic representation of a DFC architecture and a tighter packing of randomly oriented strands can be achieved in a given volume. For example, in this study we found out that if out of plane orientation was not assigned the maximum strand volume fraction would only depend on length and width aspect ratio and for strands with aspect ratio of 3 the maximum strand volume fraction would be limited to around 40%. Thus, the architecture of DFC in this study is generated using a layer by layer approach having out-of-plane oriented strands within each layer, as shown in Fig.2(a). Where the height of each layer is twice the thickness of individual strand. In DFC the out-of-plane orientation of strands depends upon the thickness of strand i.e. thin strands have less out of plane orientation as compared to thick strands. In order to mimic this physical reality in the code out-of-plane orientations of strands are approximated using a three-point interpolated spline. This is achieved by dividing the RVE in a fixed number

of layers based on the thickness of RVE "T_{RVE}" and the thickness of individual strand "S_T" i.e. $N_L = T_{RVE}/2S_T$. Thus, the strand thickness "S_T" and length "S_L" as shown in Fig. 2(b) automatically defines the out of plane path of strands. Where, the path "ABC" represents the out-of-plane curvature of strand and vertical height "AC" represents the total height of curvature, which is equal to the thickness of strand. Each layer is further divided into upper and lower regions, as shown in Fig.2(c). For each new strand generated, the intersection checks were performed separately in both regions using the hypothetical boundary boxes, shown in dotted lines in Fig.2(c) before it was added into a layer. The layer thickness in real DFC's is not uniform, e.g. Ko et al. [32] found that due to random distribution of strands, there are regions where number of strands are more than the average number of strands required to achieve the desired thickness. This tighter packing of strands in these regions results in the layers being squashed and these regions have at least 20% less thickness than that expected from a UD composite made from similar pre-preg. Based on this Ko et al.[32] suggested that the thickness of plies be reduced from cured ply thickness of a continuous UD prepreg of similar type of material. In order to account for this reduced thickness, in our code, although it is possible to use different thickness for each strand, we assume a uniformly reduced strand thickness across the RVE, for ease of implementation and because we did not have experimental data to guide a varying thickness assignment in different regions. The reduction of thickness of strands will inevitable result in lateral expansion of the strands, which means that their width will increase. Calculating an accurate increase in the width requires the knowledge of Poisson's ratio of the prepreg as it deform during the curing process. In our work we have used a simplified way of approximating the lateral expansion and the strands are assumed to deform with an equal ratio as the change in thickness as we expect the deformation to take place entirely in uncured stage.

The pseudo-code given in Fig.3 explains the overall model generation process. The user needs to define RVE dimensions, strands dimensions, number of layers and number of bins of DFC. The bins are hypothetical regions or sectors within each layer of RVE, as shown in Fig.2(d). The reason for assigning these bins is to ensure a systematic way of inserting strands that allows for completely populating a region of RVE before moving to the next. In the absence of the bin, a larger number of code iterations will be required to achieve the given volume fraction. The developed code populates the RVE layer by layer and generates strands with random position (x, y) and in-plane orientation (θ) in one of the bins within a layer of RVE. It then checks for intersection with all previously generated strands. As explained in the Fig.2(c) the intersection checks are performed for both upper and lower regions of the strands. If no intersection is detected in both the upper and lower region, using separate axis theorem (explained in section 3.2) then the strand is added into the bin being considered. The process is then

repeated for the next randomly positioned and oriented strand within that bin. If, however, an intersection is detected in either upper or lower region, then the strand is not added, and again a new randomly positioned and oriented strand is generated. This process continues until the user-specified number of iterations for that bin are completed. The code then moves to the next bin sequentially and the process is repeated until all bins in that layer are filled. After this, the same overall process is repeated for the next layer until the desired final number of layers is achieved.

With this proposed geometric modelling methodology DFC structure with any random orientations (θ) between ($0^{\circ} < \theta < 180^{\circ}$) can be produced. This can, however, be very time consuming and unnecessary because in real composites it is not expected that the properties will vary significantly if the variation in angle is less than 5º between strands. Therefore, in this paper, the orientation of strands is specified with the variation of 5° i.e. 0°, 5°, 10°…, 170°, 175°, 180°. Each angle has an equal probability of 1/37 i.e. each time a new strand is generated, and the angle is assigned, then each angle has an equal chance of selection. In the final RVE there will be some differences in the frequency of the strands at certain angles, due to the requirement of interface detection, and this results in more realistic architecture of DFC. Fig.4. shows an example of a material architecture generated through this methodology. The DFC, in this case, has been generated with only 10% fibre volume fraction and only three layers to presents an uncluttered view of the out-of-plane orientation of strands in the generated geometry. The cross-sectional view (YZ-plane) clearly shows the interlacing of strands due to the out-of-plane orientation assigned to them in each layer.

One of the key benefits of our proposed methodology is fast generation of geometric model. Thus, in term of geometry generation time the present approach is much faster, as compared to other previous models such as [30]. For example, to generate DFC architecture with 40% fibre volume fraction in a rectangular domain of 38 x 38 x 3 mm using 36 x 5.25 x 0.15 mm strands the present model takes around 20 minutes. This is much faster than the time reported in [30] which shows that their model took around 100 minutes (1 hr 40 min) to generate a similar sized RVE (38 x 38 x 3 mm) consisting of 36 mm 12k fibres for 40% fibre volume fraction. Another benefit of using this method is that the geometry generation time on average only increases linearly with increasing the size of RVE, whereas in [30] the time increases many fold for even moderate increases in RVE size (for example for 140 x 140 x 3 mm it was over 24 hrs).

The following section explains the process of checking intersection between strands.

3.2. Separate axis theorem for interface detection

SAT is used to detect the interface between two strands , according to this theorem [33], two strands do not intersect if there exists a line such that the projection of strands on the line do not intersect. This line is called a separating axis which is perpendicular to the separating line, as shown in Fig. 5(a). To ensure that two strands do not intersect each other in two-dimensional space four cases are checked to find separating line, as given by Equation (1). Fig. 5(b) shows the schematic diagram of a separate axis drawn for each case to detect an intersection between two strands. The separate axis is parallel to the unit vector along the edge of each strand. The variables used in Equation (1) are defined in the schematic diagram, see Fig. 5(c). If even one case satisfies the condition of the separating line, then strand-A and strand-B are non-intersecting strands.

$$\text{Case:1, } L||A_1;\ |T.A_1| > W_A + |(W_B B_1).A_1| + |(H_B B_2).A_1| \quad 1(a)$$

$$\text{Case:2, } L||A_2;\ |T.A_1| > H_A + |(W_B B_1).A_2| + |(H_B B_2).A_2| \quad 1(b)$$

$$\text{Case:3, } L||B_1;\ |T.B_1| > W_B + |(W_A A_1).B_1| + |(H_A A_2).B_1| \quad 1(c)$$

$$\text{Case:4, } L||B_2;\ |T.A_1| > H_B + |(W_A A_1).B_2| + |(H_A A_2).B_2| \quad 1(d)$$

where, A_1, A_2, B_1 and B_2 are the unit vectors representing the local 1-axis and 2-axis. W_A, H_A, W_B and H_B represents half of the dimensions of strand A and strand B. T represents the distance from the center of strand-A to the centre of strand-B, which is given by Equation. (2).

$$T = \sqrt{(P_{BY} - P_{AY})^2 - (P_{BX} - P_{AX})^2} \quad (2)$$

where, P_{BY}, P_{AY}, P_{BX} and P_{AX} represents the center position of the strands-A and strand-B in 2D space, with respect to global coordinate system. The projection of the centre distance (T) and the unit vectors (A_1, A_2, B_1 and B_2) on the separate axis is determined by taking their dot products. The magnitude of the projection is then compared to evaluate the presence of a separating line e.g. in Fig. 5(b) $L||A_1$ is a separating axis; whereas $L||A_2$, $L||B_1$ and $L||B_2$ are not separate axis. Hence, strand A and strand B are non-intersecting. However, if all the four cases are false than strand-A and strand-B are intersecting and there will be no separate axis or separate line.

3.3. Embedded element technique

In models where the strands geometry is modelled explicitly, FE analysis using continuous mesh methods leads to difficulties in mesh generation. It may also lead to high pre-processing and analysis (solution) time (depending on the type of elements used for continuous mesh). Embedded element approach (shell elements mesh embedded in a solid element host mesh) is a suitable alternative for such cases as it leads to both simpler mesh generation and saving of computational cost (both pre-processing and solution times) [34], [35]. This technique has been used for the prediction of elastic constants [35, 36] and stiffness/strength [37] of FRC.

Thus, in this study embedded element technique is applied which is based on mesh superposition method. In this technique strands and matrix are meshed independently and then tied together using multi-point kinematic constraints, hence it does not require any complex meshing algorithm. Moreover, the main advantage of the embedded method is that we can easily analyse the DFC structure with higher volume fraction, which is not possible using conventional meshing algorithms [38]. The embedded element scheme along with embedded and host regions is shown in Fig.6(b). In this method, the translational degree of freedoms of the host region is used to calculate the translational degree of freedoms of the embedded region using weighted averaged functions [39]. Due to the superposition of reinforcement and matrix, the additional volume of the matrix is added, this redundant volume is compensated using the stiffness reduction of reinforcement which is given by Equation. (3).

$$E_1^{emb} = E_1^s - E_m \quad 3(a)$$

$$E_2^{emb} = E_2^s - E_m \quad 3(b)$$

$$G_{12}^{emb} = G_{12}^s - E_m \quad 3(c)$$

where "E_1^s", E_2^s and G_{12}^s are the effective longitudinal, transverse and shear modulus of strands while "E_m" and "G_m" are young's modulus and shear modulus of matrix respectively.

One limitation of the technique is that it does not consider fiber/matrix interface properties explicitly, which limits the accuracy of model in term of detailed damage growth studies for interfacial failure; however, other modes can be captured with reasonable accuracy. For example, Harper et al. [30, 37] and Luchoo et al. [29] used embedded element approach to predict tensile stiffness/strength of DFC and successfully captured the effect of strands thickness and length.

3.4. Material model

In this study, the strands are modelled using a linear elastic (transversely isotropic) material model and the post-failure response is modelled as damaging elastic with failure initiation defined using the widely used Hashin failure criterion and the damage evolution is based on a model proposed by Matzenmiller et al. [40], available in ABAQUS. The elastic constants, strengths and fracture toughness of the strand materials can either be assumed same as the ply properties of UD composite made from a similar prepreg or can be derived using analytical micromechanics. These properties must be assigned to each strand in its own material coordinate system. The proposed methodology can also be applied to other cases, where the DFC may be manufactured through other processes i.e. resin transfer moulding and resin infusion, following dry fibre placement. The difference will be that the input effective properties of the strands in those cases will be determined by first considering the cured tows as UD composite chips, using an approach similar to the one described in [41]. In such

case the tow count and volume fraction with-in the strands will also be the additional required properties to estimate the input effective properties of the strands. Since, an embedded element approach is used the host region properties should also be defined, these can be taken equal to that of matrix with proper adjustment as explained in the last section. In this case the host region was assigned a homogeneous linear elastic isotropic material definition and as a modelling simplification, it is assumed that in the FE analysis the host regions will not fail. Due to this simplification, in the simulation the specimen will not fail completely as only strands will be failing. Thus, the strengths reported in this study are predicted based on a 5-10% load drop in the remote stress/strain curve obtained from the simulation.

4. Results and discussion

To demonstrate the validity of the proposed geometric modelling methodology discussed above, this section presents the comparison of stiffness and strength predictions for four different types of random DFCs with published experimental work. The strands geometry has a significant effect on the properties of the DFC, thus for the first two validation cases we have compared the results from our model to the experimental results of Selezneva et al. [12]. This is done for two different strands lengths; Case-A (long strands) and Case-B (short strands). While in the next two cases we have compared with the experimental work of Li and Peminta [27] and Li et al. [15] for two different strand thickness; Case-C (thin strand) and Case-D (thick strand). In order to carry out verification, the RVE was loaded under uniaxial tension in quasi-static conditions using ABAQUS/Explicit and in each case, the predicted tensile properties were compared with the experimental data.

4.1. Effect of strands length on the tensile stiffness and strength

In both these cases the random DFC was based on a UD carbon fibre thermoplastic prepreg, AS4/PEEK. The relevant material properties are given in Table.1. For each case, five samples of DFC were generated with achieved average strands volume fraction of 61.5±2% for the Case-A (strand length:50 mm) and 65±2.7% for the Case-B (strand length: 25 mm), where each strand is assumed to have same fibre volume fraction as present in the uncured prepreg reported in [12]. The parameters used to generate DFC architectures are mentioned in the Table.2. Selezneva et al. [42] found that thickness of strand varied between 0.139 mm to 0.071 mm, i.e. a thickness variation between 0% to 50% of the prepreg thickness. As explained in methodology section, we assume a uniform strand thickness, which in both these cases was taken equal to 0.09 mm and unlike Selezenva et al. [42] we have not ignored the expansion of strand width due to thickness reduction (Poisson's ratio effect). However, as a simplification it was assumed that the width of the strand will increase by same percentage as the reduction in height because the compression during manufacturing for real DFCs take place during uncured stage. In both

cases, each sample contains 14 layers of random strands along the thickness of RVE. It is interesting to note that due to the random packing of strands, despite the uniform thickness assumption, the strand volume fraction is neither constant in each layer nor it is constant along the in-plane dimensions (i.e. in each bin). This is desirable as it allows the model to better represent the physical reality.

The code takes around 35 minutes to generate DFC geometry of 76 x 76 x 2.5 mm consisting of 215 strands for the Case-A; from this geometric domain tensile specimens (RVE) of dimensions 75 x 25 x 2.5 mm were cut, meshed and embedded in the host domain of the same size. In Case-B the code takes around 55 minutes to generate DFC geometry of 76 x 76 x 2.5 mm consisting of 380 strands. The higher number of strands in this case was because the length of the strands was less and therefore, for every additional strand, intersection checks were performed in the upper and lower region, which results in increases in the pre-processing time. The RVE size generated from this domain in Case-B was same as the one used for Case-A.

The strands were meshed using shell element (S4), as shown in Fig.6(a), whereas matrix (host region) was meshed with 8-node solid brick elements (C3D8). The converged mesh size for strand as well as matrix regions is 1 mm (element edge length). The Fig.6(b) shows the final mesh with embedded element constraint applied between strands and matrix. Due to out-of-plane orientation of strands, the fibres orientation was aligned along the interpolated path as shown in Fig.6(c). The same Python code which generates the geometry was used to automatically assign local fibre orientation to each individual strand in the RVE. The Fig.6(d) shows the displacement boundary condition applied on each face of the RVE. The specimen is subjected to in-plane tensile loading with the displacement load applied at one end of the specimen. The resulting reaction forces and strains were recorded to generate the stress-strain curves.

The realistic morphological features of geometric model i.e. random position, random in-plane orientation and out-of-plane orientation of strands lend the reliable prediction of tensile properties. Fig.7(a) and Fig.7(b) shows the stress/strain curve of all five samples obtained from FE analysis. The variations in the predicted tensile stiffness and strength are due to the different orientation of strands in each sample, as each time a unique RVE sample was generated for the FE analysis. The stiffness and strength of DFC material depend on fibre volume fraction, the orientation of strands and frequency of strands along the loading direction. The variability of these parameters in each RVE leads to a different property analogous to what we expected in real DFC's.

To explain this phenomenon, three different specimens are selected from Fig.7(a). i.e. highest strength (A3), lowest strength (A5) and medium strength (A2). The frequency distribution of strands variation of these three samples are given in Fig.8. The orientations were divided into three groups, Region-A (strand lies between

0°- 45°), Region-B (strand lies between 50°- 130°) and Region-C (strand lies between 135°- 180°). The percentage of strands that lie in the Region-A and Region-C are mainly affecting the tensile properties. The frequency plot shown in Fig.8(a) has 62% strands in Region-A and Region-B. Hence, highest percentage of strands aligned along the loading direction, which results in the highest strength and stiffness among all samples i.e. 418 MPa and 39 GPa respectively. Whereas, sample "A2" shown in Fig.8(b) has 54% strands in these two regions (Region-A and Region-B) and exhibited medium-strength i.e. 360 MPa. On the other hand, in Fig.8(c) only 41% of the strands are aligned along the loading direction, which results in the lower strength i.e. 317 MPa.

Due to the spread of properties, it is useful to compare the average values of predicted stiffness and strength with reference values. The Table.2. shows the average predicted tensile modulus and strength in both cases along with input geometric parameters. Thus, average predicted tensile strength in the Case-A and Case-B are 365 MPa and 276 MPa, respectively, whereas the average predicted tensile modulus are 35 GPa and 27 GPa, respectively. In the case of strength prediction, the predicted tensile strengths are within the bounds of experimental data, whereas in the case of modulus prediction the present model under predicts. The COV in the strength prediction are 10% and 13%, whereas in the stiffness prediction they are 10% and 16% for the Case-A and Case-B respectively.

The main reason for the high COV is the difference in the frequency distribution and orientation of strands in each case as explained earlier. Although the variability in average strand volume fraction within each sample also plays a role, its contribution would be minor because the sample to sample variation of strand volume fraction lies within a narrow range (maximum of ±2.7%). The COV in the stiffness and strength predictions for Case-A are higher than Case-B, which indicates higher scattering of properties. This trend of COV in the strength and modulus prediction is consistent with the literature [12, 43]. It is pertinent to note that although the sample with lower strand length (lower in-plane aspect ratio) had a greater strand volume fraction (Case A: 61.5±2% vs. Case-B: 65±2.7%), the predicted strength was greater for Case A (lower strand volume fraction). This is again in keeping with the trends reported in literature and can be explained in terms of greater effective stress-transfer length for these specimens. Fig.7(c) and Fig.7(d) shows the comparison of stiffness and strength with reference values of QI laminate and that of DFC reported in [12]. This allows us to evaluate both materials and gives better visual comparison under tensile loads. The strength and stiffness values reported in Table 2, are normalized with AS4/PEEK QI laminate strength and stiffness at 60% volume fraction (QI Strength of 748 MPa and QI Modulus of 49 GPa). The graph shows that the tensile stiffness in the Case-A is 71% of QI laminate stiffness; whereas, in

the Case-B it is 57% of QI laminate stiffness. The tensile strength of both cases is between 38-48% of the QI laminate strength.

4.2. Effect of strands thickness on the tensile stiffness and strength

It has been previously reported (for example Li and Peminta [27]), that the properties of DFC are also highly sensitive to strand thickness. The methodology presented in this paper allows for exploring the cause of this property variation. Thus, in this section we present the stiffness and strength prediction comparison with the experimental work of Li and Peminta [27] and Li et al. [15]. Two cases were considered i.e. Case-C (thin strand) and Case-D (thick strand). In the Case of thin strands, the thickness of prepreg reported in [15, 27] was 0.164 mm. It was however, shown [16] that in the cured composite laminate, the thickness of strands varied and for some layers it may be up to 45% less than that of the prepreg (measured from Fig.3(b) [15]). Whereas, in the case of thick strands the prepreg thickness was reported as 0.285 mm. For the thick case, although one would expect some variation of layer thickness, it was difficult to quantify this clearly because the strands with different orientations appeared as merged or infused (Fig.3(d) [15]). Based on these observations we assumed for our model a strand thickness of 0.1 mm for Case-C (i.e. 39% reduction) and a thickness of 0.285 mm for Case-D (i.e. no reduction). As explained earlier in our model this strand thickness was used across the entire domain uniformly and as explain in previous cases width of strands were also adjusted to account for lateral expansion due to compression during manufacture. The parameters used to generate DFC architecture for the thin and thick strands are mentioned in the Table.3. Five unique DFC samples were generated, through the code and the average strand volume achieved was 60±2% and 59±2% for the Case-C and Case-D respectively. For Case-C (thin strands), the code took on average 40 minutes to generate DFC domain of 76 x 76 x 2.11 mm having around 256 strands. And it took 15 minutes to generate the DFC domain of 76 x 76 x 2.44 mm for Case-D (thick strands) which had around 90 strands. In both cases the tensile specimens (RVE) of the size mentioned in Table 3, were extracted from the respective domains and meshed using a similar strategy to the one used in earlier cases. In these cases, the random DFC was based on a UD carbon fibre thermoset prepreg, HexPly-M77. The relevant material properties are given in Table.1. Note that the input material properties of strands (elastic constants and strength) given in this table were calculated using simplified rule of mixture based on the difference in the fibre volume fraction in prepreg and that in the cured HexPly-M77 as suggested by the authors in [27].

The Fig.9(a) and Fig.9(b) shows all the stress/strain curves predicted by the model for the Case-C and Case-D. The maximum tensile predicted by the model is 264 MPa for the Case-A and 186 MPa for the Case-D, which are within the experimental bounds in comparison with reference data. The COV in the strength prediction

for Case-C and Case-D are 14% and 7% respectively, whereas the COV in the stiffness prediction is 14% and 16% respectively. The variation in the COV are consistent in comparison with experimental data. The Table.3. shows the average tensile stiffness and modulus predicted by the present model for both cases. The average tensile strength and modulus predicted by the model for the Case-C and Case-D are 218 MPa and 170 MPa respectively, and 38.5GPa and 28.5GPa respectively. Fig.9(c) and (d) shows the comparison of strength and stiffness prediction from the present model with the experimental work by Li et al. [15]. The results show that the model consistently under predicts the strength for the case of thin strands (Case-C) and it consistently under predicts the stiffness for thick strands (Case-D). Thus, overall the proposed geometric model is conservative in its prediction for these cases. Further investigation is however required to fully understand the reason behind this trend. Given the fact that we are using published experimental data, we have significant uncertainty about some of the input parameters such as reported volume fraction and true degree of randomness achieved in experimental samples; thus it is difficult to make a definite assessment in this case.

4.3. Other material architectures

One advantage of the proposed methodology is that it is easily extendable to other wide range of architectures which generally fall under one of the three categories, i.e. very thin DFC veils and gelcoats, thick DFC with random/tailored/aligned orientations and hybrid DFC's. Although the proposed methodology has been primarily validated for prepreg based random DFC in this paper. Here, in this section we will show results to demonstrate that the same methodology with little change of parameters can be used to generate other types of DFCs such as tow based aligned DFC, tailored DFC and hybrid DFC. Thus, Fig.10(a-c) shows the frequency plots of different types of thick DFC architectures generated using proposed methodology and by simply controlling the input degree of randomness allowed in the code. Similarly, by simply specifying a different level of randomness in each layer the same code was modified to generate geometric model of hybrid DFC, with random core and oriented plies on the top and bottom surface, as shown in Fig.10(d). Thus, the proposed methodology can be used to generate any DFC architecture in a 3D space. The subject of other material architectures such as hybrids is currently in progress and the results will be validated and discussed in our future publications.

5. Conclusion

A new geometric modelling methodology and FEA strategy has been proposed in this work to characterize any DFC. An algorithm has been developed that builds a 3D RVE based on explicit representation of strands within the RVE using shell elements. The code ensures non-penetration and non-intersection of strands through the use of separate axis theorem and achieves maximum volume fraction by allowing for interlacing of strands, through out of plane orientation of strands. The developed code has the capability to generate DFC

architecture with variable length of strands, thickness and volume fraction, thus allowing for a realistic RVE. The code is much faster than previous algorithms and has been demonstrated to generate meso-level RVE with realistic high strands volume fraction (up to 65±3%). Following the generation of a geometric model, FEA is performed using an embedded element technique and failure prediction within the framework of continuum damage mechanics to predict tensile stiffness and strength. The finite element results give satisfactory approximation of the predicted strength and stiffness and were used to compare the variation in the properties of random DFC for different lengths of strands and thickness. Overall, the present model is conservative in term of both stiffness and strength prediction; however, in both cases the maximum values are within the bounds of experimental data scatter. The study demonstrates that the proposed methodology is successful in virtually investigating various alternate material configurations for tailoring the response of DFC. In this paper, we have validated the strategy for both thermoset and thermoplastic based DFCs. Our methodology is generic and can be easily extended to both in-plane and out-of-plane multi-material hybrid composites. This is the focus of our ongoing work and will be presented in subsequent publications.

Acknowledgments

The authors would like to acknowledge the financial support of Universiti Teknologi PETRONAS, Malaysia to carry out this research work.

Conflicts of interest

The authors declare no conflict of interest with respect to the research or publication of this work.

References:

[1] Such M, Ward C, Potter K. Aligned discontinuous fibre composites: a short history. Journal of Multifunctional Composites. 2014;2(3):155-68.
[2] Lessard H, Lebrun G, Benkaddour A, Pham X. Influence of process parameters on the thermostamping of a [0/90] 12 carbon/polyether ether ketone laminate. Composites Part A: Applied Science and Manufacturing. 2015;70:59-68.
[3] Dodwell T, Butler R, Hunt G. Out-of-plane ply wrinkling defects during consolidation over an external radius. Composite Science and Technology. 2014;105:151-9.
[4] Feraboli P, Gasco F, Wade B, Maier S, Kwan R, Salmon W, et al. Lamborghini "forged compoiste®" techcnology for the suspension arm of Sesto Elemento. Proceedings of the 26th ASC technical conference, Montreal, Canada. 2011.
[5] Yu H, Potter KD, Wisnom MR. A novel manufacturing method for aligned discontinuous fibre composites (High Performance-Discontinuous Fibre method). Composites Part A: Applied Science and Manufacturing. 2014;65:175-85.
[6] Chang IY, Pratte JF. LDF™ thermoplastic composites technology. Journal of Thermoplastic Composite Materials. 1991;4(3):227-52.
[7] Eguemann N, Giger L, Roux M, Dransfeld C, Thiebaud F, Perreux D. Compression moulding of complex parts for the aerospace with discontinuous novel and recycled thermoplastic composite materials. 19th International Conference on Composite Materials. 2013.
[8] Koniuszewska AG, Kaczmar JW. Application of polymer based composite materials in transportation. Progress in Rubber, Plastics and Recycling Technology. 2016;32(1):1.

[9] Boursier B, Lopez A. Failure initiation and effect of defects in structural discontinuous fiber composites. Soc Adv Mater Process Eng Technical Conference. 2010.
[10] Wu M, Centea T, Nutt S. Compression molding of reused in-process waste–effects of material and process factors. Advanced Manufacturing: Polymer Composites Science. 2018;4(1):1-12.
[11] Longana ML, Yu H, Jalavand M, Wisnom MR, Potter KD. Aligned discontinuous intermingled reclaimed/virgin carbon fibre composites for high performance and pseudo-ductile behaviour in interlaminated carbon-glass hybrids. Composites Science and Technology. 2017;143:13-21.
[12] Selezneva M, Lessard L. Characterization of mechanical properties of randomly oriented strand thermoplastic composites. Journal of composite materials. 2016;50(20):2833-51.
[13] Wan Y, Takahashi J. Tensile and compressive properties of chopped carbon fiber tapes reinforced thermoplastics with different fiber lengths and molding pressures. Composites Part A: Applied Science and Manufacturing. 2016;87:271-81.
[14] Yamashita S, Hashimoto K, Suganuma H, Takahashi J. Experimental characterization of the tensile failure mode of ultra-thin chopped carbon fiber tape-reinforced thermoplastics. Journal of Reinforced Plastics and Composites. 2016;35:1342-52.
[15] Li Y, Pimenta S, Singgih J, Nothdurfter S, Schuffenhauer, Manufacturing. Experimental investigation of randomly-oriented tow-based discontinuous composites and their equivalent laminates. Composites Part A: Applied Science Manufacturing. 2017;102:64-75.
[16] Visweswaraiah SB, Selezneva M, Lessard L, Hubert P. Mechanical characterisation and modelling of randomly oriented strand architecture and their hybrids: A general review. Journal of Reinforced Plastics and Composites. 2018;37(8):548-80.
[17] Feraboli P, Peitso E, Deleo F, Cleveland T, Stickler PB. Characterization of prepreg-based discontinuous carbon fiber/epoxy systems. Journal of reinforced plastics and composites. 2009;28(10):1191-214.
[18] Nakashima Y, Yamashita S, Zhang X, Suganuma H, Takahashi J. Analytical modelling of the behaviour and scatter of the flexural modulus of randomly oriented carbon fibre strand thermoplastic composites. Composite Structures. 2017;178:217-24.
[19] Feraboli P, Cleveland T, Stickler P, Halpin J. Stochastic laminate analogy for simulating the variability in modulus of discontinuous composite materials. Composites Part A: Applied Science and Manufacturing. 2010;41(4):557-70.
[20] Toyoda H, Suganuma H, Yamashita S, Hayashi T, Fujita M, Takahashi J. Influence of strand dimension and dispersion method on rigidity and its scatter of hat shaped specimens made of randomly-oriented CFRTP strands. 21st International conference on composite materials. 2017.
[21] Halpin J, Pagano N. The laminate approximation for randomly oriented fibrous composites. Journal of Composite Materials. 1969;3(4):720-4.
[22] Selezneva M, Roy S, Lessard L, Yousefpour A. Analytical model for prediction of strength and fracture paths characteristic to randomly oriented strand (ROS) composites. Composites Part B: Engineering. 2016;96:103-11.
[23] Chen Z, Huang T, Shao Y, Li Y, Xu H, Avery K, et al. Multiscale finite element modeling of sheet molding compound (SMC) composite structure based on stochastic mesostructure reconstruction. Composite Structures. 2018;188:25-38.
[24] Qu P, Wan Y, Bao C, Sun Q, Fang G, Takahashi J. A new numerical method for the mechanical analysis of chopped carbon fiber tape-reinforced thermoplastics. Composite Structures. 2018;201:857-66.
[25] Gibson RF. Principles of composite material mechanics, chapter 6, section 6.4: CRC press; 2011.
[26] Visweswaraiah SB, Lessard L, Hubert P. Interlaminar shear behaviour of hybrid fibre architectures of randomly oriented strands combined with laminate groups. Composite Structures. 2017;176:823-32.
[27] Li Y, Pimenta S. Development and assessment of modelling strategies to predict failure in tow-based discontinuous composites. Composite Structures. 2019;209:1005-21.
[28] Visweswaraiah SB, Selezneva M, Lessard L, Hubert P. Mechanical characterisation and modelling of randomly oriented strand architecture and their hybrids – A general review. Journal of Reinforced Plastics and Composites. 2018;37(8):548-80.
[29] Luchoo R, Harper L, Warrior N, Dodworth A. Three-dimensional numerical modelling of discontinuous fibre composite architectures. Plastics, Rubber and Composites. 2011;40(6-7):356-62.

[30] Harper L, Qian C, Luchoo R, Warrior N. 3D geometric modelling of discontinuous fibre composites using a force-directed algorithm. Journal of Composite Materials. 2017;51(17):2389-406.
[31] Pan Y, Iorga L, Pelegri AA. Numerical generation of a random chopped fiber composite RVE and its elastic properties. Composites Science and Technology. 2008;68(13):2792-8.
[32] Ko S, Yang J, Tuttle ME, Salviato M. Effect of the platelet size on the fracturing behavior and size effect of discontinuous fiber composite structures. Composite Structures. 2019;227.
[33] Huynh J. Separating axis theorem for oriented bounding boxes. 2008.
[34] Kennedy RH, Terziyski JM. Experiences with Embedded Elements in Tire Modeling. In: Proceedings of ABAQUS Users' Conference. Boston, MA USA, Conference, Conference 2004. p. 13.
[35] Tabatabaei SA, Lomov SV, Verpoest I. Embedded element method in meso-finite element modeling of textile composites. CompTest 2013-Book of Abstracts. 2013:25.
[36] Tabatabaei SA, Lomov SV, Verpoest I. Assessment of embedded element technique in meso-FE modelling of fibre reinforced composites. Composite Structures. 2014;107:436-46.
[37] Harper LT, Qian C, Turner TA, Li S, Warrior NA. Representative volume elements for discontinuous carbon fibre composites – Part 1: Boundary conditions. Composites Science and Technology. 2012;72(2):225-34.
[38] Qian C, Harper L, Turner T, Li S, Warrior N. Determination of the size of representative volume elements for discontinuous fibre composites. 18th International conference on composite materials. 2011.
[39] Abaqus V. 6.14 Documentation, Section 35.4.1. Dassault Systemes Simulia Corporation. 2014.
[40] Matzenmiller A, Lubliner J, Taylor R. A constitutive model for anisotropic damage in fiber-composites. Mechanics of materials. 1995;20(2):125-52.
[41] Choudhry RS, Khan KA, Khan SZ, Khan MA, Hassan A. Micromechanical modeling of 8-harness satin weave glass fiber-reinforced composites. Journal of composite materials. 2017;51(5):705-20.
[42] Selezneva M, Roy S, Meldrum S, Lessard L, Yousefpour A. Modelling of mechanical properties of randomly oriented strand thermoplastic composites. Journal of Composite Materials. 2016;51(6):831-45.
[43] Feraboli P, Peitso E, Cleveland T, Stickler PB, Halpin JC. Notched behavior of prepreg-based discontinuous carbon fiber/epoxy systems. Composites Part A: Applied Science and Manufacturing. 2009;40(3):289-99.
[44] Tiefenthaler M, Stelzer PS, Chung CN, Reisecker V, Major Z. Characterization of the Fracture Mechanical Behavior of C-Smc Materials. Acta Polytechnica CTU Proceedings. 2018;18.

Figures:

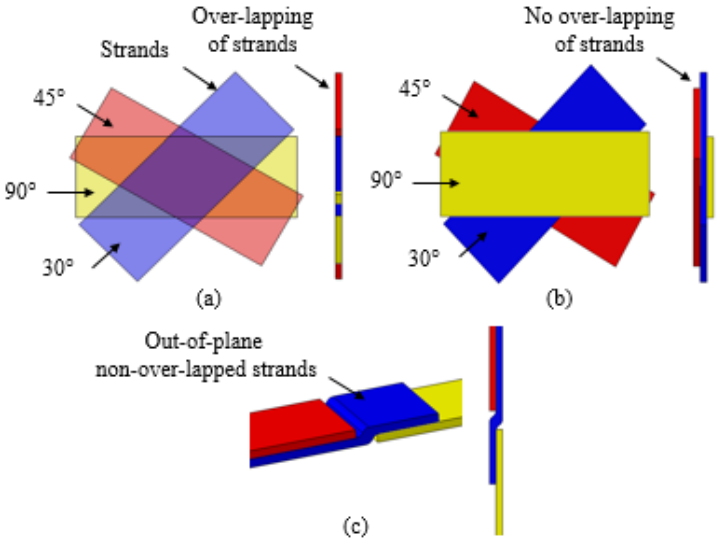

Fig.1. Types of DFC geometric models. (a) Over-lapped geometric models
(b) Non over-lapped in-plane geometric models and (c) Non over-lapped out-of-plane geometric models

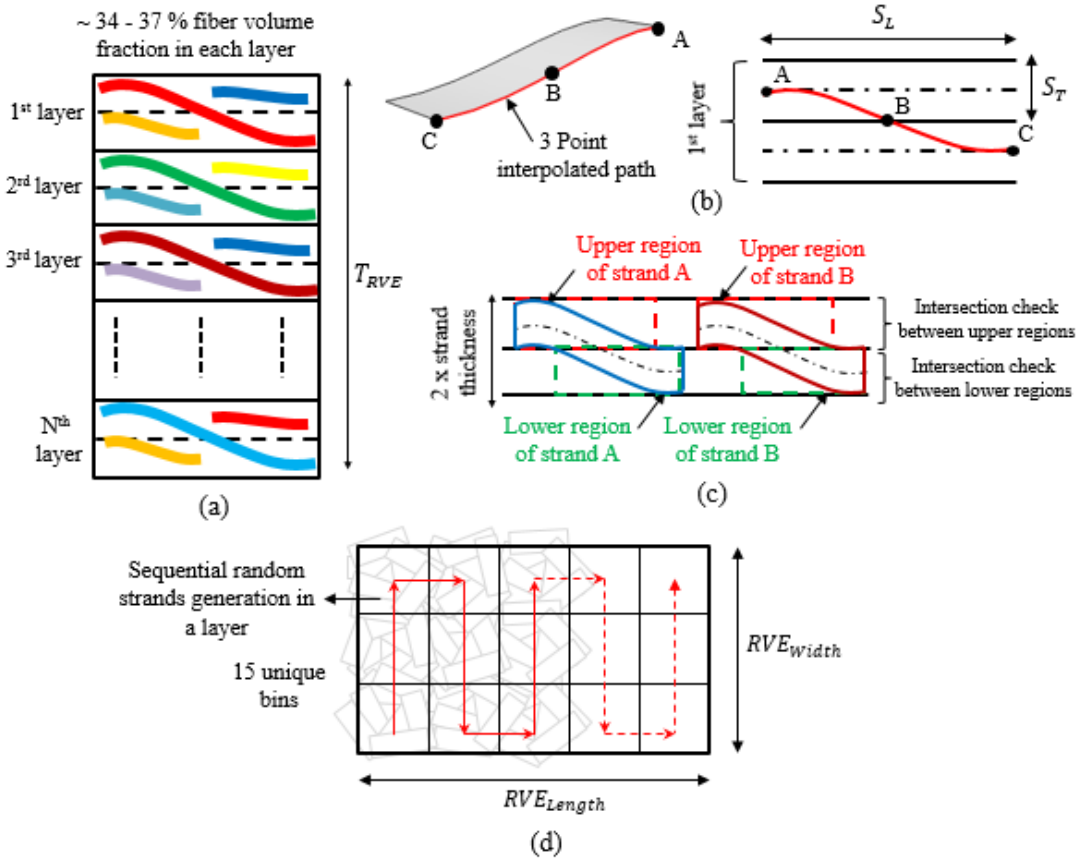

Fig.2. Schematic diagram of layered geometric model of DFC (a) Pre-defined three-point interpolated path based in strand thickness, strand length = ABC, out-of-plane curvature = AC (b) Intersection detection scheme between strands, (c) DFC layered geometric model and (d) Sequential random strands generation in a layer

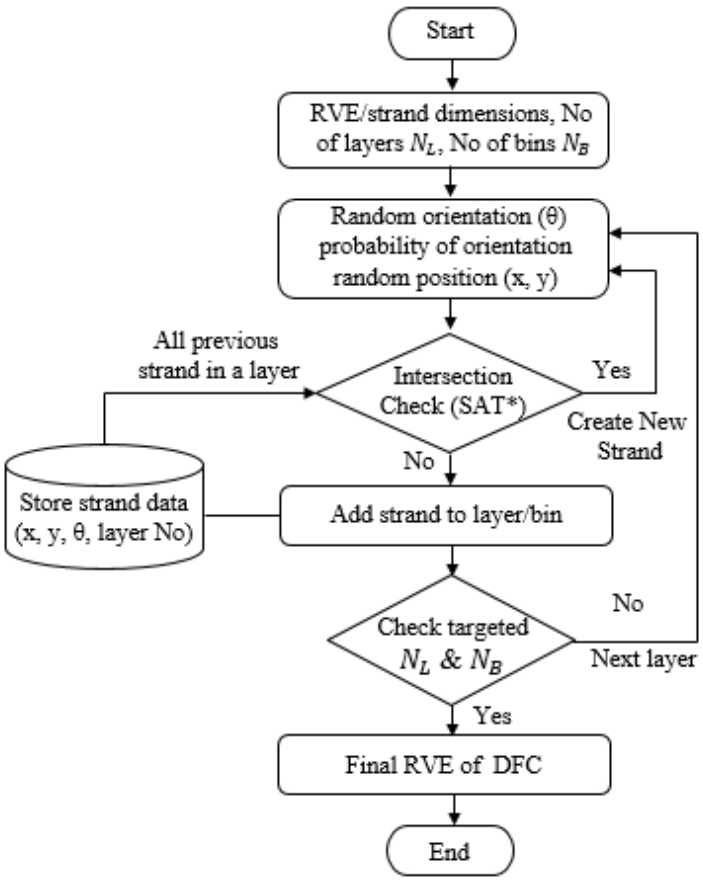

Fig.3. The pseudo code of the algorithm. (*Intersection check was perform between upper regions and lower regions of strands)

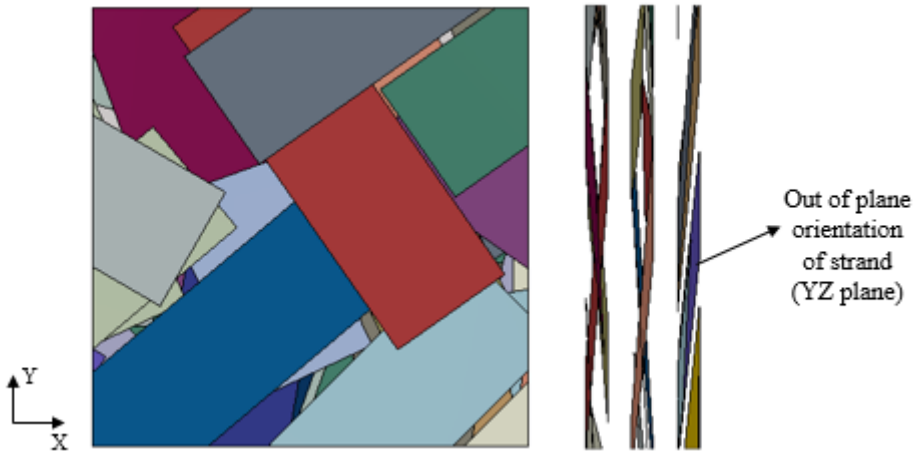

Fig.4. Out-of-plane orientation of strands in RVE. (a) 40 x 40 x 3 mm domain with 12 x 36 mm long fiber bundle, strand volume fraction = 10 %

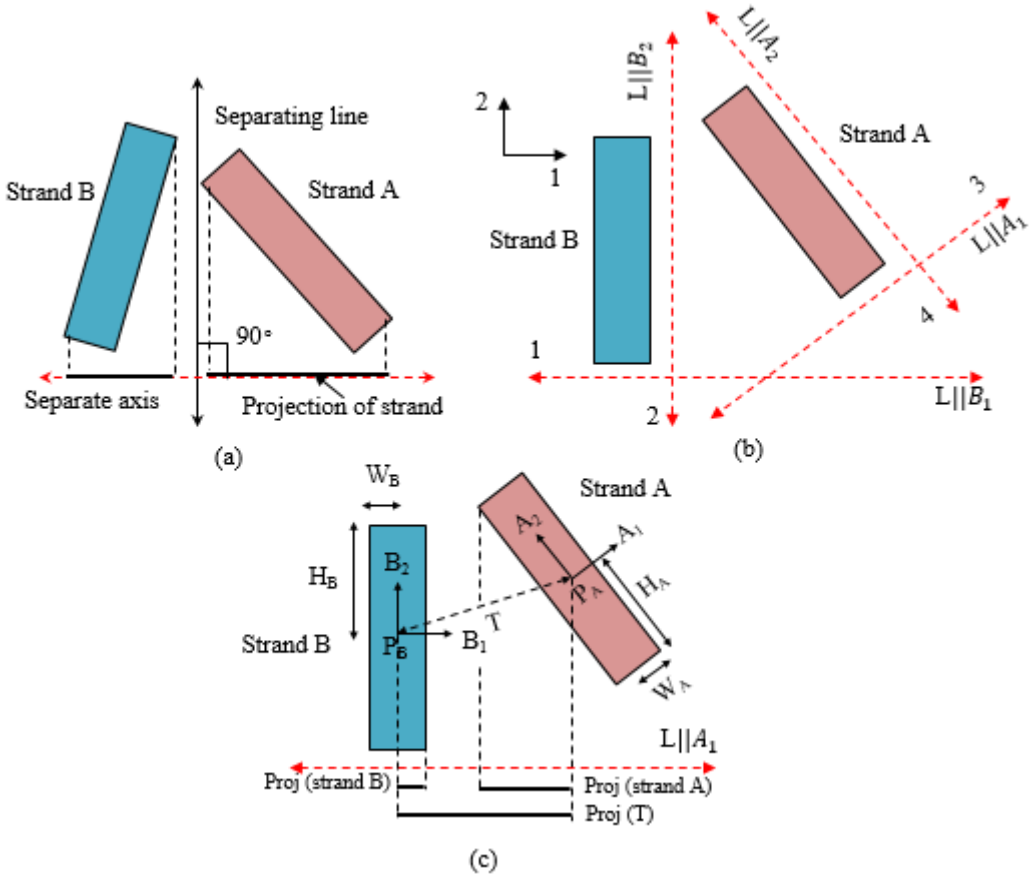

Fig.5. Schematic diagram of SAT, (a) separate axis between two strands, (b) four cases for in-plane intersection detection, (c) parameters of strands

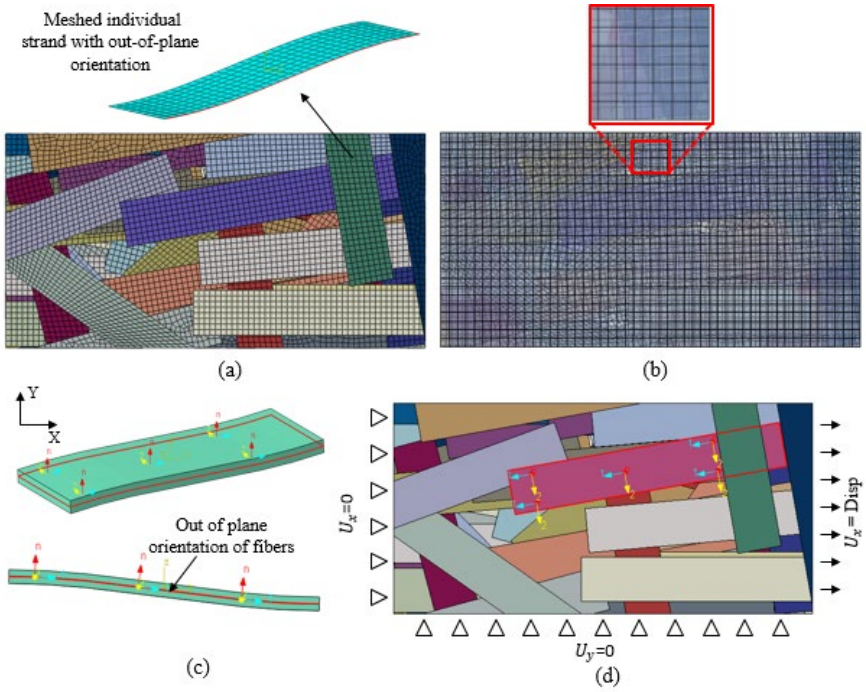

Fig.6. FE model of DFC (a) mesh strands region, (b) embedded element mesh, (c) fibre orientation in individual strand (d) geometry of DFC with boundary conditions

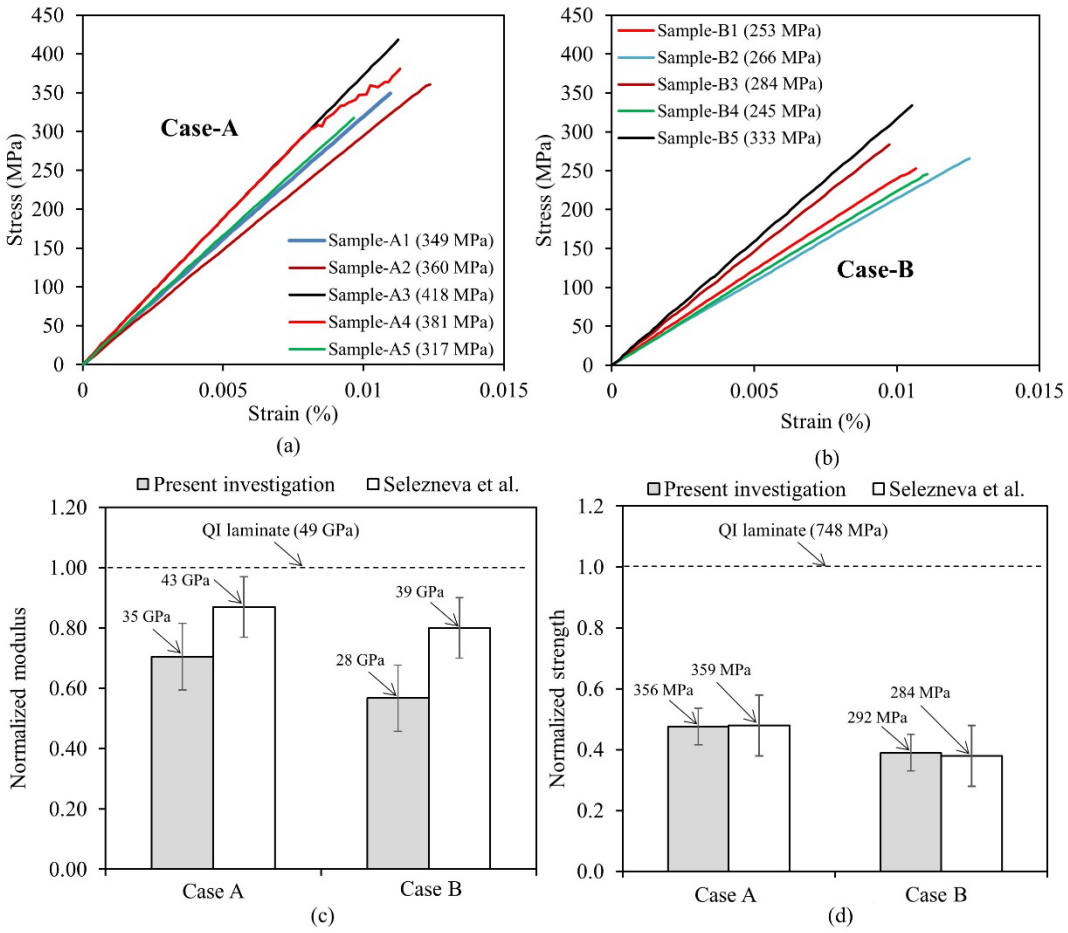

Fig.7. Strength and stiffness prediction of DFC made from AS4/PEEK UD prepreg and comparison (present model vs Selezneva et al. [12]) for DFC with two different strand lengths: Case-A 50 mm and Case-B 25 mm. (a) Stress/strain curve Case-A, (b) Stress/strain curve Case-B, (c) normalized stiffness comparison and (d) normalized strength comparison. Note: both strength and stiffness of DFC were normalized for 60% strand volume fraction against QI laminate [$0^0/\pm45^0/90^0$].

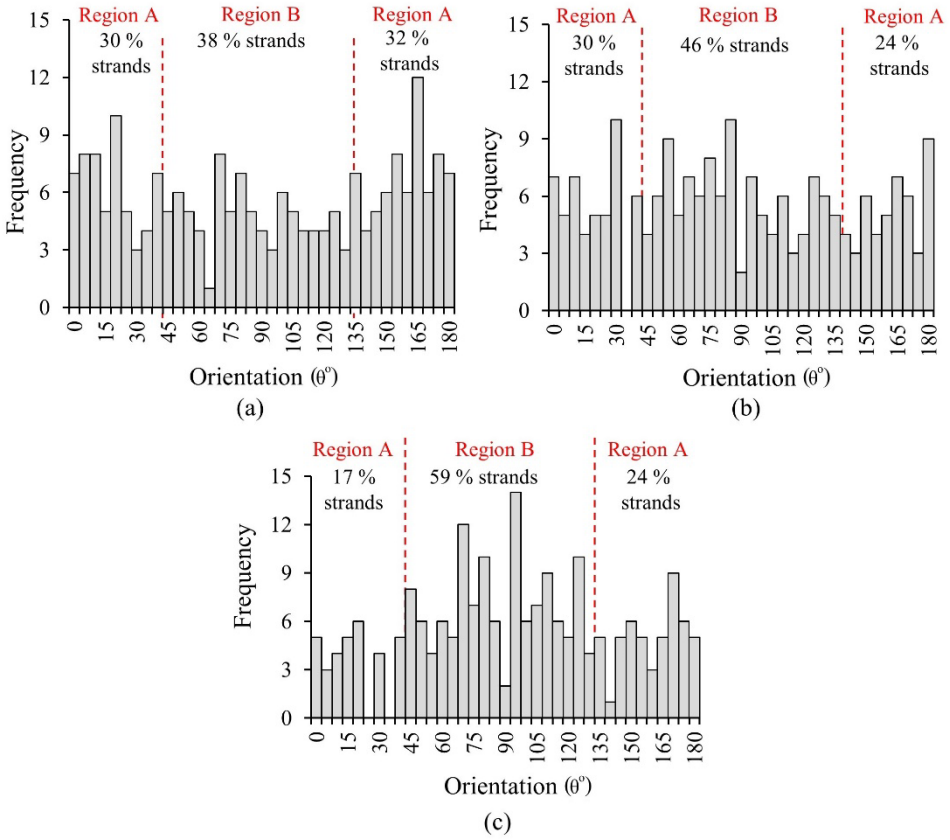

Fig.8. Frequency distribution plots, (a) sample A3 (418 MPa), (b) sample A2 (360 MPa) and sample A5 (317 MPa)

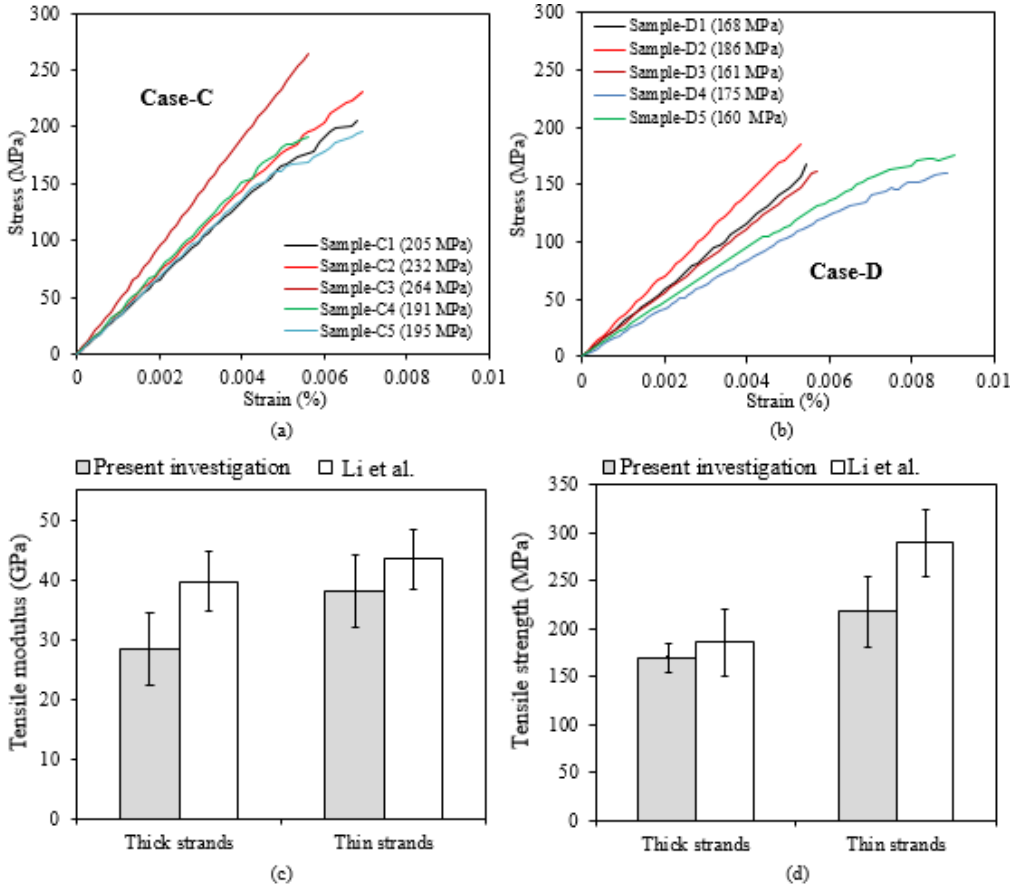

Fig.9. Comparison of strength and stiffness prediction of DFC made of HexPly-M77 carbon/epoxy prepreg (present model vs. Li et al.[15]) for DFC with two different strand thickness: Case-C (thin strand) and Case-D (thick strand) (a) Stress/strain curve Case-C, (b) Stress/strain curve Case-D, (c) Stiffness comparison and (d) Strength comparison.

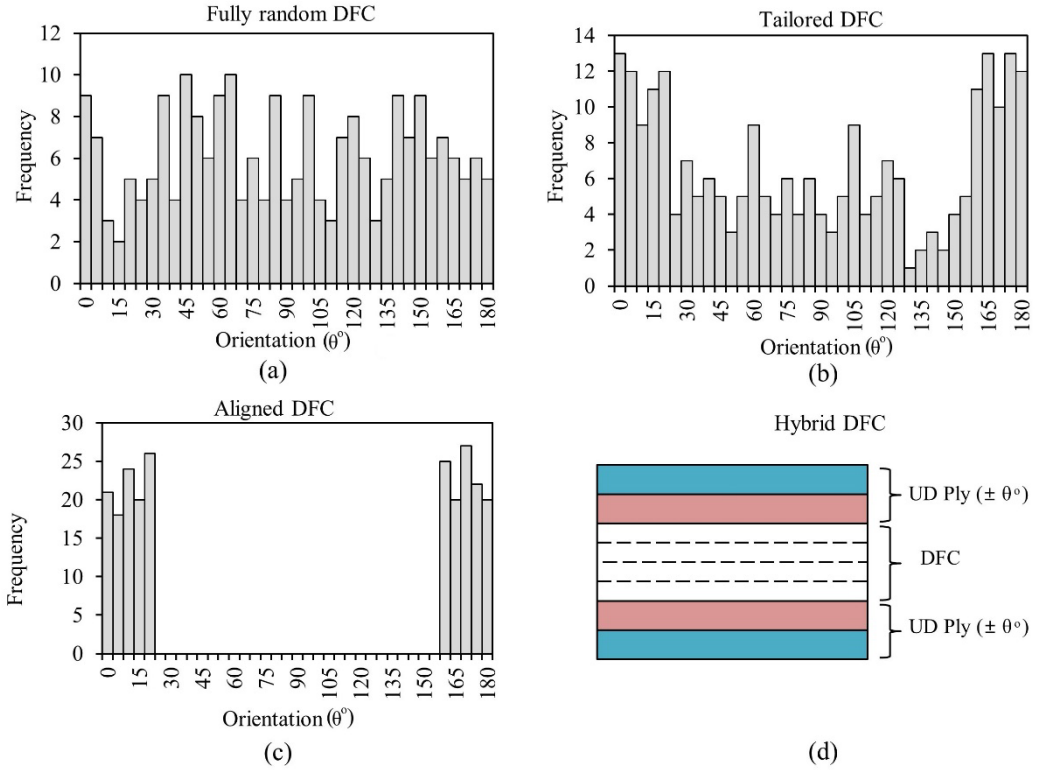

Fig.10. Types of DFC architectures that can be generated using proposed methodology. (a) fully random DFC, (b) tailored DFC, probability of (0°, ±5°, ±10°, ±15°, ±20°) have been increased, (c) aligned DFC, following angles are considered (0°,±5°, ±10°,±15°,±20°) and (d) hybrid DFC

Table.1. Properties of unidirectional composite used as an input. (a = Adjusted values to compensate redundant matrix volume)

Material	Description	Properties
Strand Properties AS4/PEEK [22]	Engineering Constants	E_1= 130 GPa (E_1^a = 126.3 GPa), E_2= 10 GPa (E_2^a = 6.3 GPa), G_{12}= 5.2 GPa (G_{12}^a = 3.85 GPa), V_{12} = 0.33
	Strengths	X_T= 2280 MPa, X_C= 1300 MPa, Y_T= 86 MPa, Y_C= 86 MPa, S_L= 152 MPa
	Fibre volume fraction	V_f = 60 %
	Average thickness of prepreg	0.139 mm
	Fracture energies	$\Gamma_{11}^T = 1\ N/mm$, $\Gamma_{11}^C = 1\ N/mm$, $\Gamma_{22}^T = 10\ N/mm$, $\Gamma_{22}^C = 10\ N/mm$
Matrix properties PEEK	Engineering Constants	E_m= 3.7 GPa, G_m= 1.35 GPa, V_m= 0.37
Strand Properties HexPly-M77 [27]	Engineering Constants (Thin strands)	E_1= 134.5 GPa (E_1^a = 131 GPa), E_2= 10.4 GPa (E_2^a = 6.9 GPa), G_{12}= 5.6 GPa (G_{12}^a = 4.29 GPa), V_{12} = 0.33
	Engineering Constants (Thick strands)	E_1= 129.9 GPa (E_1^a = 126.5 GPa), E_2= 10.08 GPa (E_2^a = 6.6 GPa), G_{12}= 5.6 GPa (G_{12}^a = 4.29 GPa), V_{12} = 0.33
	Strengths (Thin strands)	X_T= 1313 MPa, Y_T= 84.7 MPa, Y_C= 232 MPa, S_L= 90.5 MPa
	Strengths (Thick strands)	X_T= 1265 MPa, Y_T= 81.7 MPa, Y_C= 224 MPa, S_L= 87.3 MPa
	Fibre volume fraction	V_f = 51.3 %
	Average thickness of prepreg (thin case)	0.164 mm; Average thickness of prepreg (thick case): 0.285 mm
	Fracture energies [44]	$\Gamma_{11}^T = 1.83\ N/mm$, $\Gamma_{11}^C = 1.83\ N/mm$, $\Gamma_{22}^T = 3.13\ N/mm$, $\Gamma_{22}^C = 3.13\ N/mm$
Matrix properties M77	Engineering Constants	E_m= 3.45 GPa, G_m= 1.31 GPa, V_m= 0.31

Table.2. Geometry parameters and predicted tensile strength and modulus (by changing aspect ratio of strands)

Cases	Strands size (mm)	RVE size (mm)	Number of layers	Total Strands volume (%)	Strength (MPa)	Modulus (GPa)
Case-A	50x16.25x0.09	75x25x2.5	14	61.5(±2.1)	365 (±50)	35 (±4.5)
Case-B	25x16.25x0.09	75x25x2.5	14	65 (±2.7)	276 (±44)	27 (±5.5)

Table.3. Geometry parameters and predicted tensile strength and modulus (by changing thickness of strands)

Cases	Strands size (mm)	RVE size (mm)	Number of layers	Total Strands volume (%)	Strength (MPa)	Modulus (GPa)
Case-C (Thin strand)	50x11.1x0.1	75x25x2.5	12	60 (±2.2)	218 (±37)	38.5 (±6)
Case-D (Thick strand)	50x8x0.285	75x25x2.5	4	59 (±2.1)	170 (±13)	28.5 (±6)